

See discussions, stats, and author profiles for this publication at: <https://www.researchgate.net/publication/43322580>

# Application of the ReaxFF Reactive Force Field to Reactive Dynamics of Hydrocarbon Chemisorption and Decomposition

ARTICLE *in* THE JOURNAL OF PHYSICAL CHEMISTRY C · APRIL 2010

Impact Factor: 4.77 · DOI: 10.1021/jp9089003 · Source: OAI

---

CITATIONS

57

READS

51

## 5 AUTHORS, INCLUDING:



[Jonathan Edward Mueller](#)

Universität Ulm

24 PUBLICATIONS 315 CITATIONS

[SEE PROFILE](#)



[Adri C.T. van Duin](#)

Pennsylvania State University

361 PUBLICATIONS 8,214 CITATIONS

[SEE PROFILE](#)



[William A. Goddard](#)

California Institute of Technology

1,337 PUBLICATIONS 68,337 CITATIONS

[SEE PROFILE](#)

# Application of the ReaxFF Reactive Force Field to Reactive Dynamics of Hydrocarbon Chemisorption and Decomposition<sup>†</sup>

Jonathan E. Mueller,<sup>‡</sup> Adri C. T. van Duin,<sup>§</sup> and William A. Goddard III\*,<sup>‡</sup>

Materials and Process Simulation Center, California Institute of Technology, Pasadena, California 91125, and Department of Mechanical and Nuclear Engineering, Penn State University, Pennsylvania 16801

Received: September 14, 2009; Revised Manuscript Received: December 16, 2009

We report here reactive dynamics (RD) simulations of the adsorption and decomposition of a gas of 20–120 methane, ethyne, ethene, benzene, cyclohexane, or propene molecules interacting with a 21 Å diameter nickel nanoparticle (468 atoms). These RD simulations use the recently developed ReaxFF reactive force field to describe decomposition, reactivity, and desorption of hydrocarbons as they interact with nickel surfaces. We carried out 100 ps of RD as the temperature is ramped at a constant rate from 500 to 2500 K (temperature programmed reactions). We find that all four unsaturated hydrocarbon species chemisorb to the catalyst particle with essentially no activation energy (attaching to the surface through  $\pi$  electrons) and then proceed to decompose by breaking C–H bonds to form partially dehydrogenated species prior to decomposition to lower order hydrocarbons. The eventual breaking of C–C bonds usually involves a surface Ni atom inserting into the C–C bond to produce an atomic C that simultaneously with C–C cleavage moves into the subsurface layer of the particle. The greater stability of this subsurface atomic C (forming up to four Ni–C bonds) over adatom C on the particle surface (forming at most three Ni–C bonds) is critical for favorable cleaving of C–C bonds. For the two saturated hydrocarbon species (methane and cyclohexane), we observe an activation energy associated with dissociative chemisorption. These results are consistent with available experimental reactivity data and quantum mechanics (QM) energy surfaces, validating the accuracy of ReaxFF for studying hydrocarbon decomposition on nickel clusters.

## 1.0. Introduction

Nickel is the primary catalyst in the steam reforming process<sup>1</sup> for converting methane and water into synthesis gas (carbon monoxide and hydrogen) which is then used in such important industrial processes as the Haber Bosch synthesis of ammonia and the Fischer–Tropsch formation of higher hydrocarbons.<sup>2</sup> In addition, nickel catalysts are used in high temperature solid oxide fuel cells using hydrocarbon fuels, and more recently nickel has been used to catalyze the formation and growth of carbon nanotubes (CNTs) from hydrocarbons.<sup>3</sup> These applications have stimulated numerous studies of hydrocarbon rearrangements on nickel, resulting in a good understanding of the fundamental processes of simple hydrocarbon molecules reacting on low index surfaces of nickel.<sup>4–7</sup> Nevertheless, there remain many questions about the chemistry on the defect rich surfaces of nanoparticles, used, for example, as catalysts for growing CNTs.

During CNT growth, the nickel particle catalyst is responsible for catalyzing at least three processes: decomposition of the hydrocarbon feedstock, transport of the activated hydrocarbon species to the edge of the growing nanotube, and addition of the activated carbon species to the growing end of the nanotube. Each of these steps could play a rate limiting role depending on the growth conditions; however, experimental evidence suggests that feedstock decomposition is the limiting step for low temperature (350 °C) CNT growth.<sup>8</sup>

While the adsorption and decomposition of hydrocarbons on low index surfaces has been examined in many experiments<sup>2,4,7,9–12</sup> there has been little in the way of application of these results to larger catalytic problems, such as the role of feedstock decomposition in CNT growth. Thus, surface science studies of hydrocarbon chemisorption and decomposition on low index nickel surfaces try to limit the number of defects, whereas a nickel catalyst particle used in CNT growth may have many surface defects not present on the perfect (111) surface. These defects likely play important roles in catalyzing reactions on the particle surface, but experimental studies of CNT growth typically cannot isolate just one part of the process (feedstock decomposition) from the subsequent rearrangements, making it difficult to obtain a detailed chemical mechanism including the key steps involved in feedstock decomposition. We show here that reactive dynamics (RD) simulations provide mechanistic information about these heterogeneous catalytic processes, which we expect to be useful for understanding more complex reactions, such as CNT growth.

Here, we present RD simulations of six representative hydrocarbon species (methane, ethyne, ethene, benzene, cyclohexane, and propene) as they chemisorb and decompose on a 468 atom nickel nanoparticle (21 Å diameter). These six examples were chosen to cover a variety of hydrocarbon types. Ethyne and ethene allow us to compare the reactivity for species with one or two  $\pi$  bonds. Propene allows us to consider the effect of the weak allylic C–H bond. Benzene brings in effects of aromaticity and ring structures. For the saturated hydrocarbons methane and cyclohexane, we can examine the initial CH bond cleavage for systems that do not chemisorb strongly. With the exception of propene, the chemisorption and decomposition

<sup>†</sup> Part of the “Barbara J. Garrison Festschrift”.

\* Corresponding author. E-mail: wag@wag.caltech.edu.

<sup>‡</sup> California Institute of Technology.

<sup>§</sup> Penn State University.

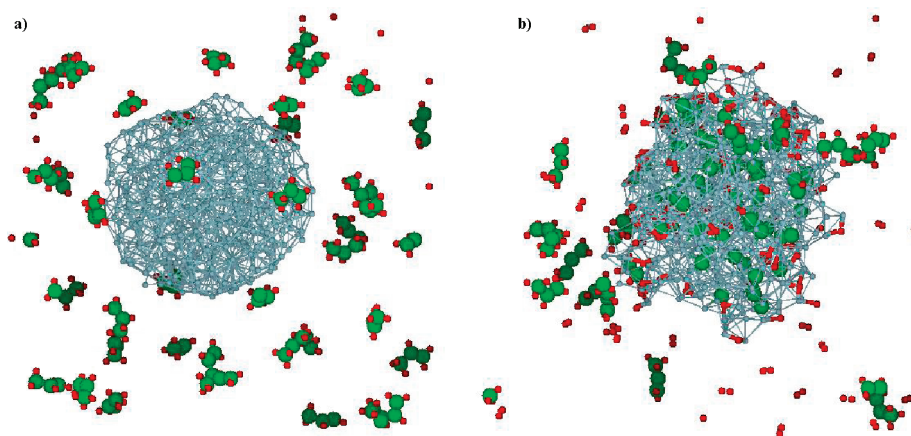


**Figure 1.** (a) Initial and (b) final structures for ReaxFF RD simulations of propene adsorption and decomposition on a nickel particle.

of each of these hydrocarbon species on nickel has been studied experimentally.<sup>2,4,7,9–12</sup> The aim of this study is to gain insight into the preferred decomposition pathways for each hydrocarbon species on nickel, in order to help guide the choice of optimum hydrocarbon feedstock species for controlling CNT growth.

## 2.0. Theoretical Methods

Modern quantum mechanics (QM) methods have been most valuable in providing reaction surfaces for reactions of simple molecules on low index surfaces.<sup>13</sup> However, studies of the reaction dynamics at higher temperatures and pressures for realistic sizes of metal clusters require system sizes and time scales well beyond the current practical limits of QM calculations. A prime example is the growth of carbon nanotubes (CNTs) from the decomposition of various hydrocarbons on catalyst nanoparticles. Nevertheless, potential energy surfaces for reactions on low index surfaces studied in typical QM studies and the comparison of these results to surface science experiments provide useful data for validating the methods suitable for larger scale studies of reaction pathways on nanoparticle surfaces. The ReaxFF reactive force field, which was trained to accurately describe hydrocarbon chemistry on Ni(111), provides a tool to extend the first principles accuracy of QM for studying the decomposition of hydrocarbon species on nickel catalyst particles.

**2.1. ReaxFF Reactive Dynamics.** The ReaxFF reactive force field potential developed recently<sup>14,15</sup> was used for all simulations (energy minimization and RD) described herein. Our temperature programmed RD simulations used the velocity Verlet integrator with a time step of 0.25 fs. The temperature was set to an initial temperature of 500 K and increased every time step at a constant rate of 20 K/ps, leading to a final system temperature of 2500 K after 100 ps. We used a Berendsen thermostat with a damping constant of 100 fs for temperature control. The temperature control achieved as well as the stability of the simulations attests to the reasonableness of these parameters for treating these particular systems.

In order to observe chemical reactions within a computationally practical simulation time, we considered a temperature range extending beyond normal experimental conditions. We expect that these elevated temperatures may affect the observed reaction pathways in two ways.

- First, the form of the Arrhenius expression for the rates results in a higher proportion of high energy processes compared with low energy processes at elevated temperatures. Thus, while the same reaction pathways are preferred

at both high and low temperatures, the preference for low energy pathways is enhanced at low temperatures.

- Second, changes in the structure of the catalyst surface at high temperature may have additional effects on reaction barriers and rates. These effects are less predictable. Nevertheless, ReaxFF RD calculations comparing CH<sub>3</sub> dissociation on hot (single increasing thermostat for nickel slab and hydrocarbons) and cold (separate increasing thermostat for hydrocarbons and constant cold thermostat for nickel slab) nickel slabs suggest that while the additional defects present on hot surfaces increase the reaction rates, there is no major change in which reaction pathways are preferred.<sup>14</sup>

We constructed the 468 atom, 21 Å diameter nickel nanoparticle by removing the corners of a 500 atom, fcc nickel cube and optimizing the structure (energy minimization). This particle diameter is within the range of catalyst particle dimensions responsible for synthesizing SWCNTs.<sup>16</sup> The hydrocarbon molecules were added at random positions in the 80 Å × 80 Å × 80 Å periodic cubic simulation cell, with at least 3.0 Å of separation from other atoms in the cell. Then, the full system was minimized (to remove any residual bad contacts) to within 0.5 kcal/mol Å rms force. The number of hydrocarbon molecules in the gas phase was chosen so that each simulation had 120 carbon atoms. Thus, the simulation of methane decomposition began with 120 methane molecules, while the simulation of benzene began with 20 benzene molecules.

Each RD simulation was initiated using a Boltzmann distribution of velocities at 500 K. During the RD, the molecules chemisorb on the surface, decompose, and sometimes desorb (e.g., H<sub>2</sub>). To obtain information about these reactive processes, we analyzed the RD trajectory to identify the molecular species at each step (using a bond-order cutoff of 0.30 to determine connectivity). The population of each chemical species (both gas phase and surface populations) was monitored as a function of time, providing a measure of the evolution of each catalytic system. The initial and final structures for the case of propene are illustrated in Figure 1. The full trajectory files (every 0.1 ps for the full 100 ps) are available as Supporting Information.

The elementary chemical reactions were extracted from the RD to obtain a reaction network indicating the transformations of various intermediates over the course of the simulation. The relative number of times that various reaction pathways are followed provide clues about the relative kinetics of various mechanistic steps.

To illustrate the importance of the catalytic activity of the nickel particle, consider the RD on 40 propene molecules (one of the more reactive species studied here) in our simulation cell, without the nickel particle. The only reaction to take place was that one molecule of propene ( $C_3H_6$ ) lost an  $H_2$  molecule to form a single propyne ( $C_3H_4$ ) molecule. This reaction took place in the final quarter of a ps of the reaction as the temperature approached 2500 K. This provides strong confirmation of the important catalytic role played by the nickel particle.

**2.2. Kinetic Model for Chemisorption.** To obtain a quantitative picture of the chemisorption rate, we use kinetic theory to derive an expression for the number of molecules in the gas phase and then obtain effective chemisorption barriers by fitting the resulting kinetic expression to our data. We derive the appropriate rate expression for chemisorption as follows:

The change in the number of molecules ( $N$ ) in the gas phase can be written in terms of the rates of adsorption ( $R_a$ ) and desorption ( $R_d$ ) from the particle surface:

$$\frac{dN}{dt} = -NR_a + (N_s)R_d \quad (1)$$

where  $N_s$  is the number of molecules chemisorbed to the surface. If the rate of desorption is negligible, we can ignore the second term so that:

$$\frac{dN}{dt} = -NR_a \quad (2)$$

We expect the rate of chemisorption to be proportional to the product of the collision rate with the surface (which is proportional to the average molecular velocity,  $\bar{v}$ , and hence to the square root of the temperature,  $\sqrt{T}$ ), the probability of having enough energy to overcome the reaction barrier (which is proportional to the Boltzmann factor,  $e^{-E_a/k_B T}$ ), and the fraction of the surface sites which are unoccupied, and hence available for reaction (which is proportional to  $M - N_s$ , where  $M$  is the total number of surface sites occupied at monolayer coverage and  $N_s$  is the number of molecules already adsorbed to the surface). Writing  $M = M - N_0$ , where  $N_0$  is the initial number of gas phase molecules, the rate equation becomes

$$\frac{dN}{dt} = -N(M + N)\Lambda\sqrt{T}e^{-E_a/k_B T} \quad (3)$$

where the constant  $\Lambda$  includes all other factors. Assuming a constant rate of temperature increase and changing variables to  $\tau = E_a/k_B T$  separates the variables, leading to

$$\frac{dN}{N(N + M)} = -A\tau^{-5/2}e^{-\tau} d\tau \quad (4)$$

where the pre-exponential factor is  $A = \Lambda(dt/dT)(1/k_B^3 E_a^5)^{1/2}$ . Integrating both sides leads to

$$\ln\left(\frac{N(M + N_0)}{N_0(M + N)}\right) = -\frac{3AM}{4}\left\{\sqrt{\pi} \operatorname{erf}\left(\sqrt{\frac{E_a}{k_B T_0}}, \sqrt{\frac{E_a}{k_B T}}\right) + e^{-E_a/k_B T}\sqrt{\frac{k_B T}{E_a}}\left(1 - \frac{2k_B T_0}{E_a}\right) - e^{-E_a/k_B T_0}\sqrt{\frac{k_B T_0}{E_a}}\left(1 - \frac{2k_B T_0}{E_a}\right)\right\} \quad (5)$$

where  $N$  is the instantaneous number of gas phase molecules and  $T$  is the instantaneous temperature  $T$  ( $T_0 = 500$  K is the initial  $T$ ).

We estimate  $M$  as follows: The catalyst particle is approximately spherical with a radius of 11 Å, leading to a surface area of 1521 Å<sup>2</sup>. An alternate estimate of the surface area is the solvent accessible surface, which is 1750 Å<sup>2</sup> (using a probe radius of 4.0 Å). We assume that the particle surface is similar to the Ni(111) surface, which leads to 5.41 Å<sup>2</sup> per 3-fold site, indicating that the cluster has about 280 3-fold surface sites. As described in the various sections, this information is used to estimate  $M$  for each hydrocarbon species investigated.  $N$  as a function of time from RD simulations is used to calculate the left-hand side of eq 5. Then, the  $A$  and  $E_a$  parameters are fit to the right-hand side to the data (least-squares fit using the solver in Microsoft Excel<sup>17</sup>).

### 3.0. Results and Discussion

**3.1. Chemisorption and Decomposition. 3.1.1. Methane (Figure 2).** Methane is the most studied hydrocarbon species for nickel catalyzed decomposition and reforming reactions. Chemisorption requires breaking a C–H bond, leading to  $CH_3$  and H radical fragments that each chemisorb onto the surface. We first observe these chemisorption products at  $T_A = 1300$  K (41 ps). Beyond this point, the rate of chemisorption increases superlinearly with increasing temperature, and  $CH_3$  chemisorbed to the surface begins to decompose.

Methane chemisorbed onto the nickel particle can undergo further dehydrogenation with subsequent breaking of additional C–H bonds, or it can produce higher order hydrocarbons by forming C–C bonds. We found two cases in which C–C bonds were formed in our RD. Near the end of the simulation (>93 ps and 2350 K), the reaction of two C atoms to form surface  $C_2$  occurs twice; however, only one of the  $C_2$  molecules produced survives to the end. Also, we find that two of the methyl groups react to form  $C_2H_6$  (which immediately loses one H, to form  $C_2H_5$ ) during the final 0.25 ps in the simulation when the temperature is nearly 2500 K. Thus, under our simulation conditions, C–C bonds do not form readily from the products of methane gas chemisorption.

On the other hand, a significant number of chemisorbed H atoms are produced (100 at the end), some of which desorbed to form gas phase as  $H_2$  gas (19 at the end). Because chemisorption requires breaking a C–H bond, the initial appearance of atomic chemisorbed H is simultaneous with the chemisorption of the  $CH_3$  fragment at  $T_H = T_A = 1300$  K. Once chemisorbed  $CH_3$  is present on the surface (first appears at 41 ps), it easily loses an H atom to form chemisorbed  $CH_2$  (first appears at 46 ps) and a second to form chemisorbed CH (first appears at 48 ps). The final H is more difficult to remove from chemisorbed CH, so that chemisorbed atomic C is not observed until the temperature reaches  $T_C = 1850$  K (68 ps). A visual examination of the trajectory (see the Supporting Information) suggests that the energy for breaking the final C–H bond is

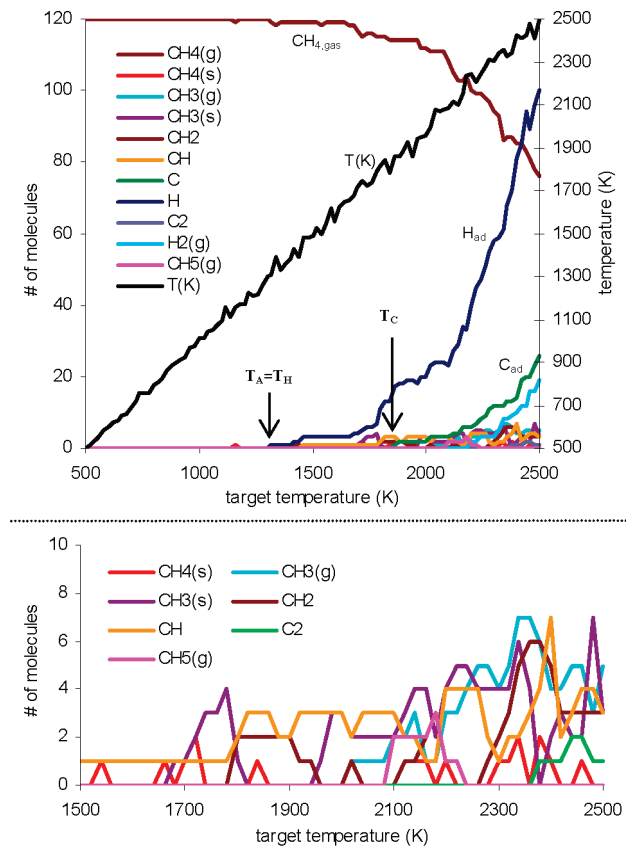


**Figure 2.** Population analysis and reaction network for methane chemisorption and decomposition on nickel. The numbers in brackets in the reaction network are the final populations of each species, and the number on each reaction arrow is the total number of times the reaction took place. The simulation started with 120 CH<sub>4</sub> gas phase molecules and no other HC species.

stabilized by migration of the C atom produced into the nickel particle subsurface. Thus, atomic C is not formed until there is sufficient thermal energy for it to migrate into the nickel particle subsurface, where it is energetically more stable.

The final population has 44 of the 120 original methane molecules chemisorbed onto the particle. Of these, 28 were completely dehydrogenated, two of which combine to form C<sub>2</sub>. The remainder of the chemisorbed methane is accounted for in adsorbed intermediates (three molecules each of CH, CH<sub>2</sub>, and CH<sub>3</sub>) and gas phase radicals (five gas phase CH<sub>3</sub> radicals and one gas phase C<sub>2</sub>H<sub>5</sub>). The presence of all three CH<sub>x</sub> intermediates highlights their similar stabilities on the surface, while the presence of the gas phase methyl radicals is an artifact of the high simulation temperature, since they appear between 2000 and 2500 K.

Several experimental<sup>7,10,18</sup> and theoretical<sup>5,6,19,20</sup> studies have focused on the products and intermediates formed as methyl decomposes on nickel. Methylidyne (CH) is the energetically favored species on Ni(111), but CH<sub>3</sub> is also observed experimentally. Methylene (CH<sub>2</sub>) readily decomposes to CH, and is not observed experimentally as an intermediate in the dehydrogenation process. Consistent with these observations, the

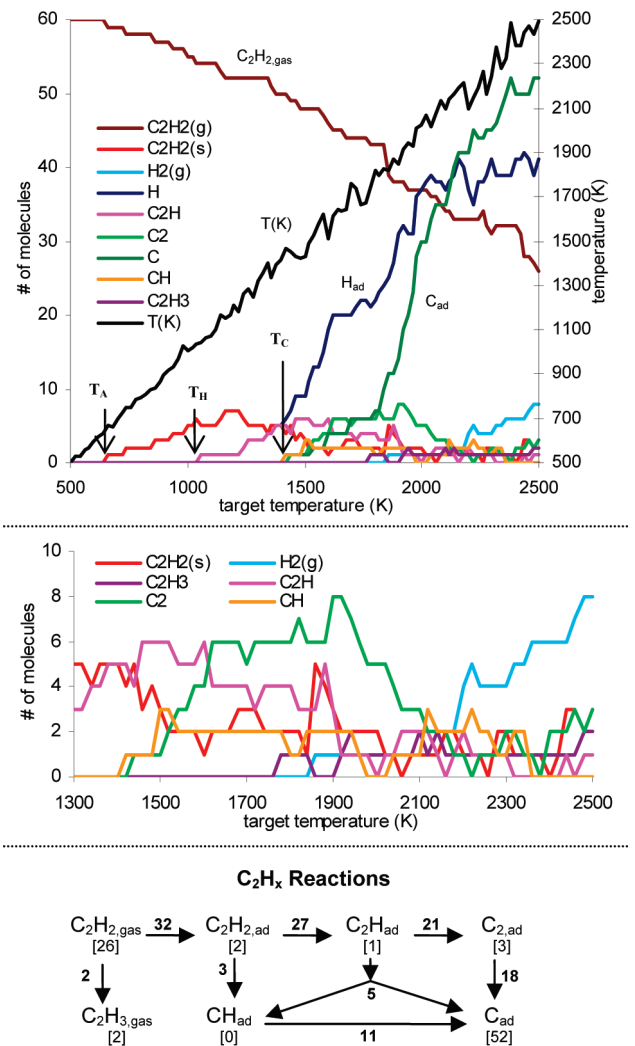


**Figure 3.** Population analysis and reaction network for ethyne chemisorption and decomposition on nickel. The numbers in brackets of the reaction network are the final populations of each species. The number on each reaction arrow is the total number of times the specific reaction took place. The simulation started with 60 C<sub>2</sub>H<sub>2</sub> gas phase molecules and no other HC species.

population of CH is typically higher than the population of CH<sub>2</sub> in our RD, although our system is far from a perfect (111) surface.

Experimental studies also show that, at moderate temperatures (between 250 and 400 K) and high surface coverage, CH dimerizes to form ethyne or even four-, six-, and eight-member rings. At higher temperatures (above 400 K), CH is reformed and eventually breaks up (by 700 K), with atomic C dissolving into the bulk. For our RD, the temperature range is too high and the coverage too low for C–C bond formation to be favorable, so we do not see such combination processes.

**3.1.2. Ethyne (Figure 3).** The two  $\pi$  bonds of ethyne (C<sub>2</sub>H<sub>2</sub>) can each be broken to form  $\sigma$  bonds as it chemisorbs to the nickel surface. Thus, ethyne is able to chemisorb onto the particle without fragmenting. Indeed, our RD finds that it first adsorbs onto the nickel particle after 8 ps, when the temperature reaches T<sub>A</sub> = 650 K.

Once adsorbed, ethyne does not begin to decompose for another 20 ps (28 ps, T<sub>H</sub> = 1050 K), at which point the adsorbed C<sub>2</sub>H<sub>2</sub> begins dehydrogenating to form C<sub>2</sub>H. The population of C<sub>2</sub>H builds for about 20 ps until it breaks down (46 ps, T<sub>C</sub> = 1450 K) to form either CH and C or C<sub>2</sub> and H. Above this

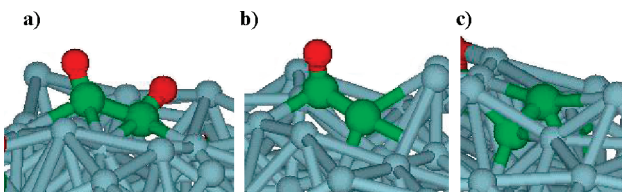


**Figure 4.** Snapshots of structures observed during ethyne decomposition on the nickel nanoparticle: (a)  $\text{C}_2\text{H}_2$  chemisorbed to the particle surface; (b)  $\text{C}_2\text{H}$  on the particle surface; (c)  $\text{C}_2$  in the subsurface region, where the C–C bond is more readily broken.

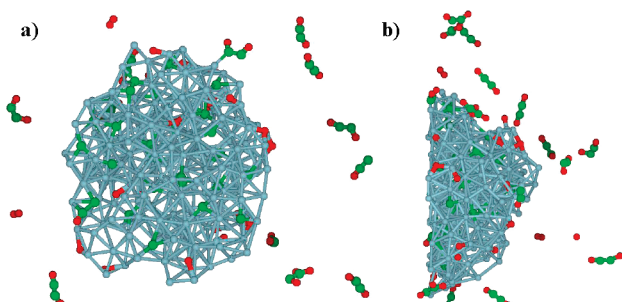


**Figure 5.** Cross section (particle and simulation cell sliced in half) of the final structure from ethyne simulation showing the migration of atomic C into the interior of the catalyst particle: (a) head on view; (b) side view.

temperature, there are typically only about two  $\text{C}_2\text{H}_2$  molecules on the surface at any given time despite continued adsorption of additional molecules from the gas phase. This indicates that above 1450 K the rate of decomposition is at least as fast as the rate of adsorption.

Similarly, the population of CH remains low, indicating that the rate of CH formation from  $\text{C}_2\text{H}$  is slower than the rate for decomposing CH into C and H. In contrast, the population of  $\text{C}_2$  is sustained between 50 and 75 ps (1500 and 2000 K), before the rate for  $\text{C}_2$  to decompose into atomic C exceeds the rate of  $\text{C}_2$  formation. Both CH and  $\text{C}_2$  decomposition produce subsurface atomic C, which shows a marked increase at 70 ps (1900 K). This corresponds to a breakdown in the structure of the nickel particle providing the newly formed C atoms an easy opportunity to migrate into the subsurface of the particle.

Snapshots (Figure 4) from the simulation suggest that  $\text{C}_2$  also migrates into the subsurface of the particle as it loses its final H, and that it is here where the C–C bond is finally broken. Thus, both  $\text{C}_2$  and atomic C are stabilized by moving into the subsurface, making the stability of subsurface C an important factor in facilitating cleavage of C–C bonds. By the end of our simulations (at a temperature of 2500 K), the atomic C formed has migrated into the bulk of the particle, as shown in Figure 5.

The RD leads to the reaction network in Figure 3 with three pathways from  $\text{C}_2\text{H}_2$  to C, corresponding to the three  $\text{C}_2\text{H}_x$  species that can be broken up into single C fragments. The vast majority (27) dehydrogenate to form  $\text{C}_2\text{H}$ , while only 3 adsorbed  $\text{C}_2\text{H}_2$  molecules break the C–C bond to form CH fragments. Similarly, while 5 of 27  $\text{C}_2\text{H}$  molecules break down into C and CH, the majority (21) lose H to form  $\text{C}_2$ , which then breaks down into subsurface atomic C. Thus, there is a marked preference for dehydrogenation prior to breaking C–C bonds, indicating that C–H bonds are easier to break on the nickel particle than C–C bonds.

Ethyne decomposition on nickel has been studied extensively experimentally.<sup>4,21–28</sup> On the (111) surface, each C of the ethyne forms a  $\sigma$  bond with adjacent 3-fold sites. Thus, one C–C  $\pi$

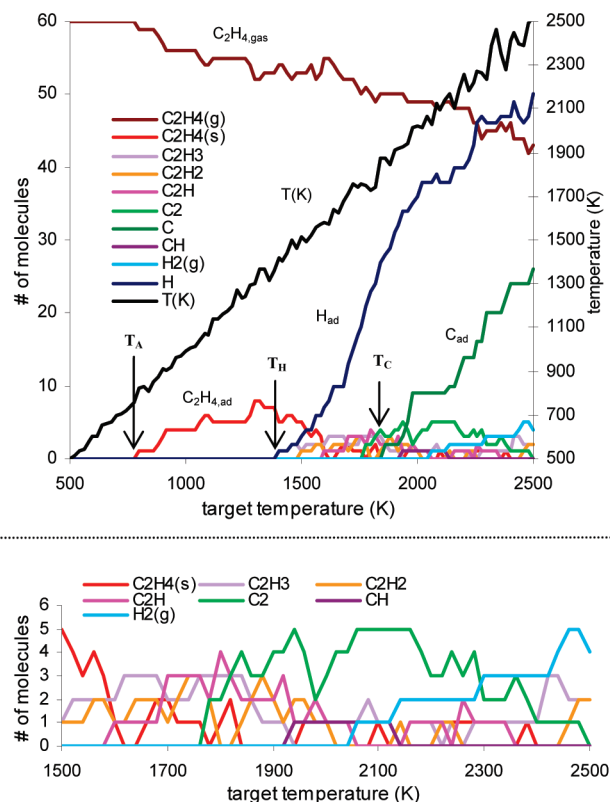


**Figure 6.** Population analysis and reaction network for ethene chemisorption and decomposition on nickel. The numbers in brackets of the reaction network are the final populations of each species, and the number on each reaction arrow is the overall number of times the reaction took place. The simulation started with 60  $\text{C}_2\text{H}_4$  gas phase molecules and no other HC species.

bond becomes two C–Ni  $\sigma$  bonds. As the temperature is increased above 300 K, this di- $\sigma$  bonded  $\text{C}_2\text{H}_2$  decomposes into two chemisorbed CH's before breaking down into atomic C and H at higher temperatures (450 K).<sup>27</sup> Thus, on the flat surface, the C–C bonds break before C–H bonds. However, the presence of steps on the Ni(111) surface lowers the activation barrier for C–H bond cleavage, accelerating the decomposition of  $\text{C}_2\text{H}_4$  to form chemisorbed  $\text{C}_2$ . Because our nanoparticle has many step-like defects, it is plausible that it behaves like the stepped surface, rather than the flat surface. Indeed, we observe C–H bonds breaking prior to C–C bonds.

Previous QM studies<sup>29–31</sup> agree with experiment<sup>21</sup> in showing that HCCH binds most strongly to a  $\mu$ -bridge site on Ni(111), with the C atoms at adjacent 3-fold positions. The close proximity of HCCH to the surface represented by this structure is in good agreement with the structures we observe in our RD.

**3.1.3. Ethene (Figure 6).** Ethene ( $\text{C}_2\text{H}_4$ ) behaves similarly to ethyne in both chemisorption and decomposition. Like ethyne, ethene can break a C–C  $\pi$  bond to form two sigma bonds to the nickel surface. We expect this process to have a low barrier, and indeed, we observe ethene chemisorbing onto the particle after 18 ps when the temperature reaches  $T_A = 800$  K.

Only half as many ethene molecules (17) chemisorbed onto the particle compared to ethyne molecules (32). Since both

ethene and ethyne have essentially no barrier to chemisorption (they both bind by breaking C–C  $\pi$  bonds) and neither leads to significant steric effects, our results suggest that ethyne has a pre-exponential factor twice as large as ethene. This is plausible since the solid angle for which ethyne pi orbitals can overlap the Ni surface atoms is about twice that for ethene.

After adsorbing to the surface,  $C_2H_4$  is stable for another 27 ps, until the temperature reaches  $T_H = 1400$  K (45 ps), at which point dehydrogenation begins, forming  $C_2H_3$ ,  $C_2H_2$ , and  $C_2H$  intermediates on the way to  $C_2$ , which first appears at 64 ps (1750 K). At these temperatures, the dehydrogenation process is fast, keeping the concentration of these  $C_2H_x$  intermediates low. At 68 ps ( $T_C = 1850$  K), C–C bonds begin to break. Here, dehydrogenation is generally completed to form  $C_2$  before the C–C bond breaks (we found only one case in which the C–C bond in  $C_2H$  is broken first). This preference is the same as observed for ethyne, which dehydrogenates completely before breaking C–C bonds.

Ethene has been studied extensively on nickel surfaces experimentally.<sup>4,21–28</sup> On the (111) surface, the C–C  $\pi$  bond is broken to form two  $\sigma$  bonds each to an on-top nickel site, with the C–C bond lying parallel to the surface. As the temperature is increased on the (111) surface,  $C_2H_4$  loses two H atoms between 200 and 230 K to form  $C_2H_2$ . This resulting ethyne then decomposes according to the pathway outlined previously.<sup>27</sup> Again, the presence of steps on the Ni(111) surface accelerates the cleavage of C–H bonds in  $C_2H_4$ .<sup>4</sup> The defect rich nature of the nanoparticle in our studies explains why we observe C–H bond breaking well in advance of C–C bond breaking.

QM calculations have been reported for ethene chemisorption on Ni(111).<sup>29–31</sup> In agreement with experiment,<sup>21</sup> these calculations find that ethene binds further away from the surface with each C atom sitting directly above a Ni surface atom. This is consistent with the structures observed in our RD.

**3.1.4. Benzene (Figure 7).** The RD simulations for benzene ( $C_6H_6$ ) show benzene initially binding through the C–C  $\pi$  orbitals to the nickel particle, leading to a geometry parallel to the surface, while retaining its resonance stabilization (Figure 8a). As a result, there is no  $\sigma$  bond as in ethene, leading to weak bonding to the surface, making the adsorption of benzene onto the nickel particle reversible so that a half dozen benzene desorption events are observed over the course of the RD simulation.

While benzene begins adsorbing to the nickel particle near the beginning of the simulation (2 ps,  $T_A = 550$  K), it does not begin to decompose until  $T_H = 900$  K (19 ps) when we observe an adsorbed  $C_6H_6$  losing H to form  $C_6H_5$ . As the temperature increases, additional dehydrogenation occurs, forming di- $\sigma$  bonded  $C_6H_4$  (45 ps, 1400 K), tri- $\sigma$  bonded allylic  $C_6H_3$  (49 ps, 1500 K), and eventually 1,2,3,4-C $_6H_2$  (63 ps, 1750 K) with four bonds to the surface. After 64 ps, at  $T_C = 1750$  K, C–C bonds begin to break as  $C_6H_3$  is converted to  $C_5H_3$ , which is then able to further decompose by breaking either C–C or C–H bonds. Throughout the simulation, we find that breaking C–C bonds usually involves breaking a single C or  $C_2$  off of a longer hydrocarbon chain while bonding it into the subsurface. In other words, when the terminal C or terminal  $C_2$  is denuded of C–H bonds, the Ni nanoparticle acts like Pac-Man,<sup>32</sup> gobbling up the terminal C or  $C_2$  but stopping at C atoms that still have C–H bonds. Except for the buildup of  $C_2$  near the end of the simulation, the populations of chains with less than six C atoms remain small, suggesting that the decomposition of C–C bonds occurs quickly once the first C has been removed from the ring.

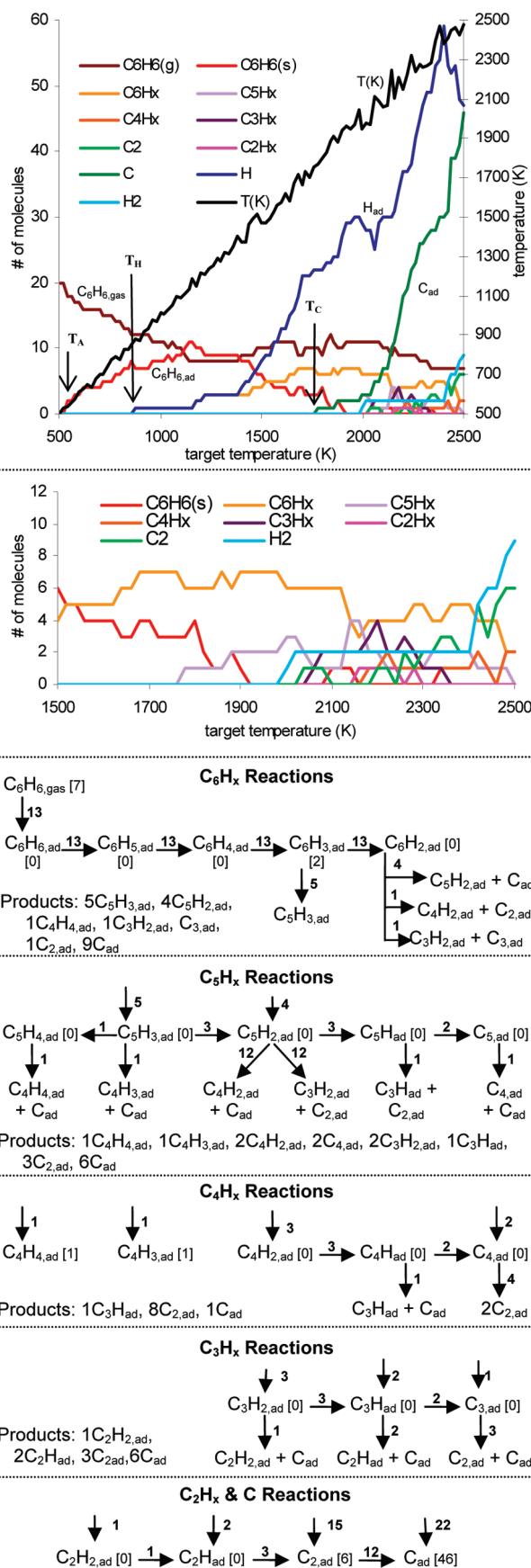


**Figure 7.** Population analysis and reaction network for benzene chemisorption and decomposition on nickel. The numbers in brackets of the reaction network are the final populations of each species, and the number on each reaction arrow is the overall number of times the reaction took place. The simulation started with 20  $C_6H_6$  gas phase molecules and no other hydrocarbon species.

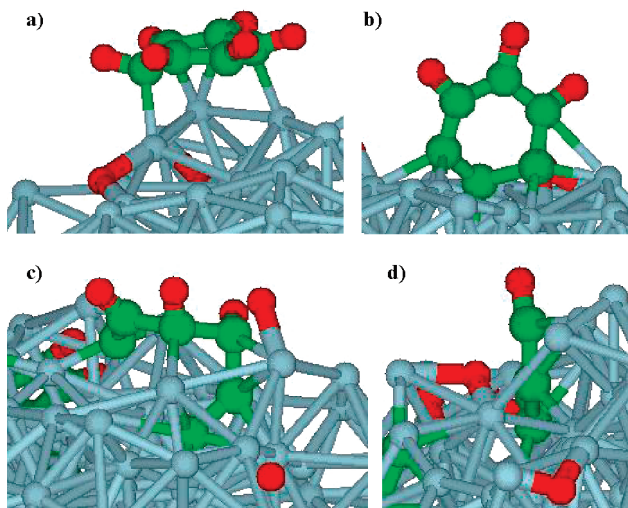


**Figure 8.** Snapshots of structures observed during benzene simulation: (a)  $C_6H_6$  chemisorbed parallel to the particle surface; (b)  $C_6H_3$  ring standing perpendicular to the surface; (c)  $C_6H_3$  chain on the particle surface with a dehydrogenated tail in the subsurface; (d)  $C_3H$  showing the preference of bare C atoms (no H) for the subsurface and hydrogenated C atoms for the surface.

The most abundant intermediates at each length are  $C_5H_3$ ,  $C_4H_2$ ,  $C_3H$ , and  $C_2$ .

An examination of snapshots from the trajectory suggests why these species are formed along the preferred decomposition pathway (Figure 8). Benzene adsorbs initially with its ring parallel to the particle surface, bonding to the surface using its  $\pi$  electrons. Breaking one C–H bond frees up a C in the ring to form a  $\sigma$  bond to the surface, which distorts the planar nature of the ring. The addition of a second  $\sigma$  bond to the surface, following the loss of another H, results in a 1,2-benzyne which bonds to the surface with the ring standing up perpendicular to the surface. In this perpendicular orientation, only two of the four remaining H atoms are close enough to the surface to react. Thus, we do not observe any  $C_6H$  or  $C_6$  in our simulation because the remaining H atoms in  $C_6H_2$  are too far from the surface to react readily.

Now that  $C_6H_4$  is perpendicular to the surface, it loses one or two of the remaining H atoms close to the surface to form allylic  $C_6H_3$  or 1,2,3,4- $C_6H_2$ . With three or four  $\sigma$  bonds to the surface, Ni atoms are now able to insert into the dehydrogenated C–C bonds. This initial cleavage of a C–C bond breaks the ring structure but not the molecule, so our current analysis does not detect it. However, breaking a second C–C bond results in the formation of two new species. Thus, 9 out of 11 reactive events involve cleavage of a C–C bond in  $C_6H_3$  or  $C_6H_2$  to form atomic chemisorbed C. Thus, like Pac-Man, the Ni particle “swallows” each C atom by migrating it into the subsurface, leaving  $C_5H_3$  or  $C_5H_2$  behind on the surface. The  $C_5H_x$  species either remains stretched out as a chain or (in at least one observed instance) reconnects to form a five-membered  $C_5H_5$  ring.

The decomposition of  $C_5H_x$  species is typically initiated from  $C_5H_2$ , resulting in loss of either C or  $C_2$  into the subsurface of the Ni particle. Cleaving a C–C bond to form two new species (rather than just breaking a ring) results in either  $C_2$  or atomic C as one of the products formed (except for one instance of  $C_6H_2 \rightarrow C_3H_2 + C_3$ ). Thus, the Ni particle catalyzes the cleavage of a C–C bond by inserting Ni atoms into the bond to introduce either C or  $C_2$  into the subsurface. Even for  $C_5H_x$  species, one or two of the H atoms are often inaccessible to the surface, so

that 6 of the 9  $C_5H_x$  decomposition events that form lower order hydrocarbons initiate immediately from  $C_5H_2$  or more highly saturated  $C_5H_x$  species.

As the cleavage of C–C bonds continues to shorten the hydrocarbon chain, the H atoms that were originally too far away from the surface to react with the Ni as part of the six-membered ring are drawn closer to the surface, allowing the cleavage of the remaining C–H bonds. As for ethyne and ethene, there is a noticeable preference for breaking off C rather than  $CH_x$  species when cleaving C–C bonds. Thus, we can think of the overall mechanism as proceeding roughly along the following lines. Because cleavage of C–C bonds is stabilized by introducing C or  $C_2$  into the subsurface of the nickel particle, the part of the hydrocarbon chain where a C–C bond is going to be attacked must first be stripped of H so that Ni atoms are able to insert into the bond and surround the C atom being introduced into the particle subsurface. As the chain length is reduced, H atoms originally too far away from the surface to react are reeled in toward the surface where they are stripped away, allowing another C–C bond to be broken. Thus, we might idealize the mechanism by considering it as proceeding iteratively:  $C_6H_6 \rightarrow C_6H_5 \rightarrow C_6H_4 \rightarrow C_6H_3 \rightarrow C_5H_3 \rightarrow C_5H_2 \rightarrow C_4H_2 \rightarrow C_4H \rightarrow C_3H \rightarrow C_3 \rightarrow C_2 \rightarrow C$ .

The interaction of benzene with nickel surfaces has been studied previously.<sup>4,9,11,12,25,33–38</sup> Benzene can be synthesized from methane on Ni(111), where it is stable up to 395 K, at which temperature it begins to desorb and dehydrogenate.<sup>12</sup> These experiments have been interpreted in terms of benzene forming  $\pi$  bonds to the surface with the carbon ring remaining flat<sup>24</sup> while the H atoms point slightly away from the surface.<sup>38</sup> This initial binding structure is in agreement with our findings.

**3.1.5. Cyclohexane (Figure 9).** Like methane, cyclohexane ( $C_6H_{12}$ ) requires a C–H bond to break in order to chemisorb onto the nanoparticle. Thus, we observe no chemisorption until the temperature reaches  $T_A = T_H = 1650$  K (59 ps), at which point chemisorption results in H and  $C_6H_{11}$  each bonding to the surface. The RD simulations reveal both initial dissociation of axial C–H bonds and equatorial C–H bonds upon chemisorption of  $C_6H_{12}$  with no obvious preference.

Once chemisorption occurs, dehydrogenation follows quickly as the predominant process. The pathways followed are analogous to those observed for benzene. As a result, dehydrogenation is observed to proceed as far as  $C_6H_2$ . Unlike benzene, cyclohexane can lose H and subsequently desorb from the surface because  $\pi$  bonds are formed when adjacent H atoms are lost. Thus, we observe two  $C_6H_{10}$  molecules, one  $C_6H_9$  molecule, and one  $C_6H_8$  molecule in the gas phase. Three of these retain their original carbon ring structure, but  $C_6H_8$  is a chain with three resonance stabilized double bonds.

Few C–C bonds are broken over the course of the simulation. The first such cleavage occurs after 88 ps at  $T_C = 2250$  K and produces  $C_4H_2$  and  $C_2$  from  $C_6H_2$ . The products further decompose into atomic C and H over the remainder of the simulation, following reaction pathways similar to those observed in the decomposition of other hydrocarbon species. The only other C–C bond to break is the conversion of  $C_6H_7$  into  $C_4H_4$  and  $C_2H_3$  in the final picosecond of the simulation. Thus, of the nine adsorbed molecules, only two convert into lower order hydrocarbons: one  $C_4H_3$ , one  $C_2H_3$ , and six C atoms. The remaining seven only undergo dehydrogenation. Of these, four return to the gas phase, as noted above, and three remain on the surface as two molecular fragments of  $C_6H_4$  and one of  $C_6H_2$ .

Experiments show that cyclohexane physisorbs to Ni(111) at 150 K and desorbs above 170 K. In the presence of steps, it

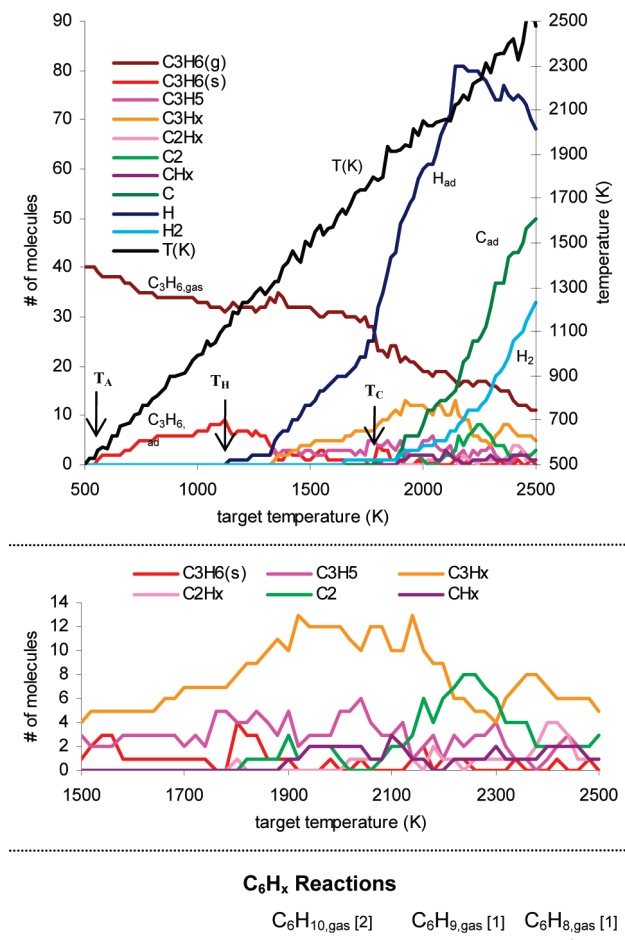


**Figure 9.** Population analysis and reaction network for cyclohexane chemisorption and decomposition on nickel. The numbers in brackets of the reaction network are the final populations of each species, and the number on each reaction arrow is the overall number of times the reaction took place. The simulation started with 20  $C_6H_{10}$  gas phase molecules and no other hydrocarbon species.

dehydrogenates to form benzene.<sup>4</sup> Since our focus is primarily on chemisorption, and we start at 500 K, there is no direct comparison with these experiments. However, the experimental observation that surface defects (particularly steps) play an important role in breaking C–H bonds is consistent with our RD study.

**3.1.6. Propene (Figure 10).** Like ethyne and ethene, propene ( $H_2C=CH-CH_3$ ) has a  $\pi$  bond allowing it to bond to the surface without breaking C–H bonds. Thus, it begins to adsorb onto the particle after only 3 ps, when the temperature reaches  $T_A = 550$  K.

Adsorbed propene ( $C_3H_6$ ) is a stable species similar to chemisorbed ethene, except with a  $CH_3$  group substituted for H. The population of  $H_2C=CH-CH_3$  on the surface grows to nine molecules over the first 31 ps ( $T_H = 1150$  K) before dehydrogenation begins. We find cases in the simulation where the first H is lost from each of the three C atoms in  $H_2C=CH-CH_3$ , to form  $HC_a-C_aH-CH_3$ ,  $H_2C_a-C_a-CH_3$ , and

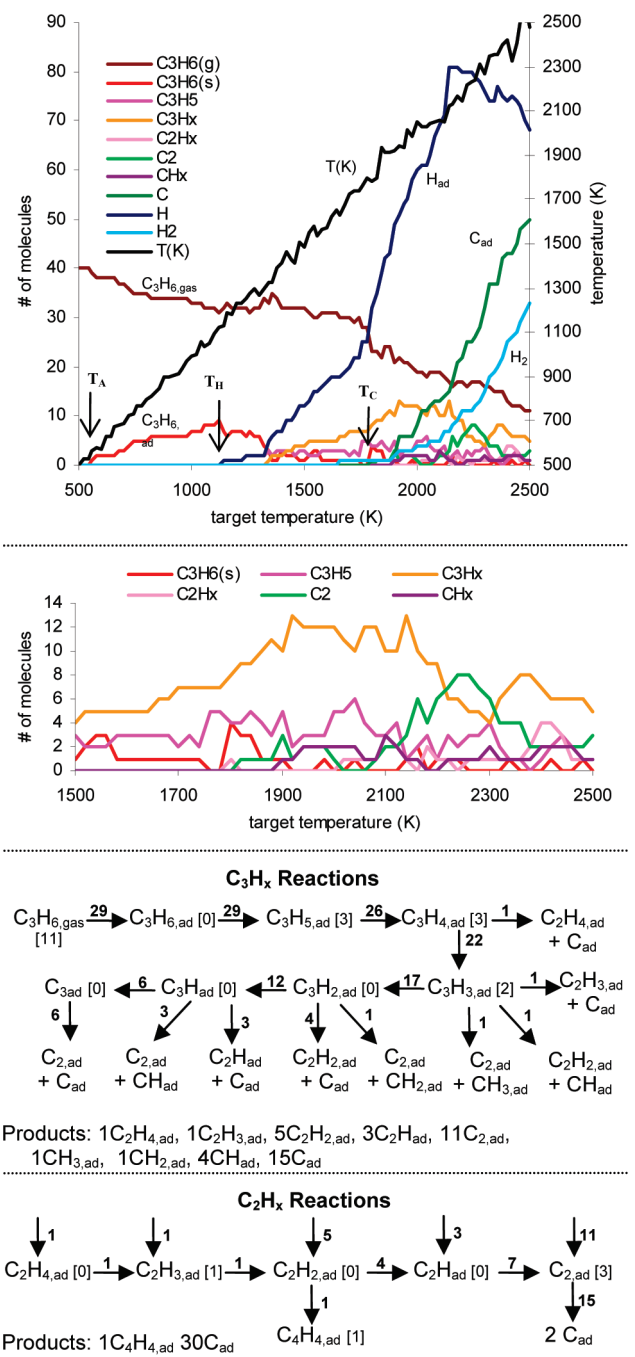


**Figure 10.** Population analysis and reaction network for propene chemisorption and decomposition on nickel nanoparticle. The numbers in brackets in the reaction network are the final populations of each species, and the number on each reaction arrow is the overall number of times the reaction took place. The simulation started with 40  $C_3H_6$  gas phase molecules and no other hydrocarbon species.

$H_2C_a-C_aH-C_aH_2$ , where the subscript a indicates which atoms are bonded to the surface. Note here that in the gas phase the allyl product would be dominant, because of resonance; however, on the surface the unpaired electrons bind to the Ni surface so that all species have similar energies. In all cases,  $C_3H_5$  further dehydrogenates to  $C_3H_4$  before any C–C bonds break. Again, we observe all forms of  $C_3H_4$  that

**TABLE 1: Results from ReaxFF RD Simulations of Hydrocarbons Adsorbing and Decomposing on a 468 Atom Nickel Particle<sup>a</sup>**

	ethyne	benzene	cyclohexane	ethene	methane	propene
$T_A$ (K)	650	550	1650	800	1300	550
$T_H$ (K)	1050	900	1650	1400	1300	1150
$T_C$ (K)	1450	1750	2250	1850	1850	1800

<sup>a</sup> The temperature was ramped from 500 to 2500 K at a rate 20 K/ps.  $T_A$ : temperature at which the first molecule adsorbs onto the nickel nanoparticle.  $T_H$ : temperature at which the first C–H bond is broken to produce atomic H on the nickel nanoparticle.  $T_C$ : temperature at which a C–C bond is broken to first produce atomic C on the nickel nanoparticle.

can be obtained from propene by breaking only C–H bonds. These are  $\text{HC}_a\text{—C}_a\text{H}\text{—C}_a\text{H}_2$ ,  $\text{HC}_a\text{—C}_a\text{—CH}_3$ ,  $\text{C}_a\text{—C}_a\text{H}\text{—CH}_3$ , and  $\text{H}_2\text{C}_a\text{—C}_a\text{—C}_a\text{H}_2$ . Further, dehydrogenation of  $\text{C}_3\text{H}_4$  is strongly preferred, leading to  $\text{C}_3\text{H}_3$ ,  $\text{C}_3\text{H}_2$ ,  $\text{C}_3\text{H}$ , and finally to  $\text{C}_3$  in 22 of 23 total reactions that start from  $\text{C}_3\text{H}_4$ . The one exception converts  $\text{C}_a\text{—C}_a\text{H}\text{—CH}_3$  into atomic C at an interstitial subsurface site and the carbine,  $\text{HC}_a\text{—CH}_3$ , bonded to the Ni surface. As dehydrogenation continues, the ratio of each  $\text{C}_3\text{H}_x$  species undergoing a C–C bond cleavage compared with further dehydrogenation increases. This is partially a function of there being fewer C–H bonds to break and partially a function of the increased ease of breaking off C or  $\text{C}_2$  compared to  $\text{CH}_x$  species. Of the 21 reactions converting  $\text{C}_3\text{H}_x$  species to  $\text{C}_2\text{H}_x$  and  $\text{CH}_x$  species, all but one result directly in the formation of either  $\text{C}_2$  or atomic C at interstitial subsurface sites. This again emphasizes the importance of forming multiple C–Ni bonds in order to stabilize breaking C–C bonds by moving C or  $\text{C}_2$  into the subsurface. Similar to ethene and benzene, atomic C is not produced by breaking C–C bonds until the temperature reaches  $T_C = 1800$  K.

**3.2. Summary of RD Results.** To compare the relative reactivities of various hydrocarbon species, it is useful to consider the temperature at which each species first adsorbs to the particle ( $T_A$ ), the temperature at which H first appears signifying the first breaking of a C–H bond ( $T_H$ ), and finally the temperature when atomic C is first produced corresponding to C–C bonds breaking and C moving into the bulk ( $T_C$ ). These results are summarized in Table 1.

First, we consider chemisorption. At  $T_A = 550$  K, propene and benzene are the first species to adsorb to the surface (through their  $\pi$  bonds). Ethyne and ethene also have  $\pi$  bonds available for bonding to the surface, and begin sticking at  $T_A = 650$  K and  $T_A = 800$  K, respectively. In contrast, methane and cyclohexane have no  $\pi$  bond electrons to form bonds with the surface, so chemisorption requires breaking a C–H  $\sigma$  bond, so that C can form a  $\sigma$  bond to the surface. This results in chemisorption being delayed until these systems reach higher temperatures:  $T_A = 1300$  K and  $T_A = 1650$  K, respectively.

Once molecules chemisorb onto the surface, dehydrogenation (breaking C–H bonds) precedes the cleavage of C–C bonds in all cases studied. There are two important considerations in understanding the different temperatures at which we first observe C–H bonds breaking in the various species. First, the initial temperature of adsorption can be limiting, because breaking C–H bonds cannot be catalyzed by the particle until the hydrocarbon is adsorbed onto the particle surface. As a result,  $T_H = 1300$  K and  $T_H = 1650$  K for methane and cyclohexane, respectively, are identical to  $T_A$  for those species because chemisorption results in H formation.

Second, because breaking the C–H bonds is catalyzed by inserting a Ni atom into the C–H bond, it occurs more readily

when the C–H bond is close to the surface. For example, adsorbed benzene with its ring structure parallel to the surface has the C–H bonds close to the surface and hence is vulnerable to dehydrogenation. Thus, we observe C–H bonds beginning to break at  $T_H = 900$  K, the lowest temperature for any of the hydrocarbons we studied. The C–H bonds in ethyne are the next most reactive as they begin to break at  $T_H = 1050$  K. Unlike benzene, where we expect the ring to sit well above the surface, ethyne binds to the surface with the C atoms in hollow sites. Thus, while the H atoms point away from the surface, the closer proximity of the C atoms to the surface enables Ni atoms to more easily insert into the C–H bond to stabilize both the C and H atoms as the bond breaks.

In contrast, steric effects require propene to sit further above the surface so that it requires a higher temperature,  $T_H = 1150$  K, before C–H bonds first break, even though the C–H bond is weaker. Methane is the next most reactive, requiring a C–H bond to break in order for the initial chemisorption step to start taking place at  $T_H = 1300$  K. The C–H bonds in the  $\text{CH}_3$  resulting from this chemisorption begin to break at 1400 K, the same temperature at which the C–H bonds in ethene begin breaking ( $T_H = 1400$  K). Finally, atomic H is not produced from cyclohexane until chemisorption begins at  $T_H = 1650$  K. In this final case, the initiation of dehydrogenation is clearly limited by the commencement of the chemisorption process.

Finally, we consider the cleavage of C–C bonds. The most common mechanism we observe for C–C bond cleavage is the Pac-Man mechanism which requires a bare C at the end of a hydrocarbon chain. In the Pac-Man mechanism, a Ni atom inserts into the C–C bond, and the C atom at the end of the hydrocarbon chain is drawn into the catalyst particle subsurface where it is stabilized by forming four bonds to Ni, rather than the three it is limited to when sitting on top of the surface. Thus, subsurface atomic C formation is the product in the vast majority of reactions involving C–C bond cleavage that we observe. As a result, we can use the temperature at which atomic C first appears as a convenient indicator of when C–C bond cleavage is initiated, allowing us to include the decomposition of methane in our comparison. In this context, the decomposition processes studied here provide the following particular insights.

The C–C bonds in ethyne begin to break at  $T_C = 1450$  K to form C and CH. The low temperature for this process relative to the other species studied is likely due to the dimensions of the molecule, which allow it to fit deeply into adjacent hollow sites on the surface. In this position, the Ni–C bonding is readily able to compensate for the C–C bond energy being lost. Furthermore, ethyne can undergo at most two dehydrogenation reactions, before the only remaining bond to break is a C–C bond, so that  $\text{C}_2$  first appears soon after the temperature reaches 1400 K. Four of the other species begin to produce C near 1800 K: ethyne at  $T_C = 1750$  K, propene at  $T_C = 1800$  K, and ethene and methane at  $T_C = 1850$  K. This temperature corresponds to the melting point of bulk Ni. Such a partially melted, amorphous particle surface makes it easier to introduce C atoms into the particle subsurface, where they are stabilized energetically to facilitate breaking a C–C bond. Cyclohexane is more difficult to decompose and does not produce C atoms (or any other species with less than six C atoms) until the temperature reaches  $T_C = 2250$  K.

**3.3. Implications for CNT Growth.** The findings of our RD study have at least three implications for understanding feedstock selection for CNT growth. First, barriers for chemisorption for saturated hydrocarbon species are significantly higher than barriers for unsaturated species. Thus, at appropriate tempera-

tures and pressures, it should be possible to reduce the hydrocarbon population on the catalyst surface by using saturated hydrocarbon feedstock. There may be growth conditions under which a less than saturated concentration of hydrocarbon in the surface would be advantageous; however, surface (and possibly subsurface or bulk) saturation is generally believed to be a requirement for CNT growth. Thus, the low chemisorption barriers of unsaturated hydrocarbon species may provide an important advantage in pursuing low temperature growth.

Second, we find that C–H bonds break far more readily than C–C bonds. The orbital arguments underlying this were explained by Goddard et al.<sup>39</sup> Thus, there may be conditions under which CNT growth occurs via the addition of short carbon chains rather than individual atoms. In particular, we observe  $C_2$  as a stable intermediate in most of the decomposition pathways studied here. Preliminary ReaxFF simulations suggest that the barrier for addition of  $C_2$  to the edge of a growing CNT may have a lower activation barrier than the addition of atomic C. If this is the case, there may be advantages to using hydrocarbon feedstock that easily breaks down into units of  $C_2$ .

Finally, the energetic favorability of subsurface C has been highlighted by the important role it plays in stabilizing breaking C–C bonds. There are models of CNT growth (particularly the VLS model) in which a nickel carbide phase is an important thermodynamic driving force for growth.<sup>40–42</sup> In this case, there may be advantages to selecting hydrocarbon feedstock that more easily decomposes to form the carbide phase. On the other hand, there is evidence that some growth conditions depend on surface, rather than bulk, migration of the activated hydrocarbon species.<sup>43</sup> Under such growth conditions, the formation of nickel carbide may not be advantageous. Here also, the choice of feedstock may play a role in determining the extent of carbide formation and its subsequent effect on the CNT growth process.

**3.3.1. Comparison with Other Theoretical Studies of CNT Growth.** Other reactive force fields have been developed for nickel (or other similar transition metals such as iron) and carbon in order to study carbon nanotube growth,<sup>44–50</sup> however, none of these studies treat hydrocarbon species. Thus, previous reactive force field studies of nanotube growth have been limited to migration and addition of the activated carbon species to the growing nanotube edge as well as nucleation steps from the activated carbon species. Because extensive QM studies of feedstock decomposition (taking into account all of the complexities of a real nanoparticle surface) are not computationally feasible with current technology, there are no previous, systematic, computational studies of hydrocarbon feedstock decomposition on catalyst nanoparticles.

Nevertheless, a variety of tight-binding, reactive dynamics and density functional theory studies have noted the greater stability of subsurface C over atomic C on nickel surfaces.<sup>49,51,52</sup> Thus, they conclude that saturating the nickel bulk (or at least the subsurface layer) may play an important role in adjusting the chemical potential of C to an appropriate level for CNT growth.

**3.4. Analysis of Chemisorption Rates.** To analyze the chemisorption rates from our RD simulations quantitatively, we utilized the kinetic model developed in section 2.2. Because this model assumes that desorption is negligible, it is not appropriate to apply it to the simulations on ethene, propene, and benzene, so we only consider methane, cyclohexane, and ethyne. The reaction barriers for adsorption obtained by fitting the kinetic model to our RD data are 41 kcal/mol for methane chemisorption, 31 kcal/mol for cyclohexane chemisorption, and

1.9 kcal/mol for ethyne adsorption. The methane result is incompatible with the calculated activation energies on Ni(111), where ReaxFF leads to 18.4 kcal/mol,<sup>14</sup> in good agreement with the experimental value of 17.7 kcal/mol<sup>2</sup> and the QM activation energy of 18.9 kcal/mol.<sup>19</sup> This invalidates the simplifying assumptions in our kinetic model, because we expect a lower barrier on a defect rich surface, similar to those observed at steps.<sup>53,54</sup> Additional details are available in the Supporting Information.

## 4.0. Conclusions

Using the ReaxFF reactive force field with the parameters for C/H/Ni developed recently,<sup>14</sup> we studied the adsorption and decomposition of six hydrocarbon species (ethyne, benzene, cyclohexane, ethene, methane, and propene) on a 468 atom nickel nanoparticle. We find that unsaturated hydrocarbons (molecules with  $\pi$  bonds) adsorb and decompose far more readily than saturated hydrocarbons (molecules with only  $\sigma$  bonds), because they chemisorb readily onto the surface with a barrier. This difference is evident in the temperature at which chemisorption is initiated in our simulations ( $T_A = 800$  K or lower for unsaturated species and  $T_A = 1300$  K or higher for saturated species). The difference may be an important factor in selecting feedstock species for low temperature CNT growth.

Once the species are chemisorbed to the particle, dehydrogenation essentially always precedes decomposition into lower order hydrocarbons. The C–C bonds essentially never break until one of the C is denuded of H at which point it can insert into the subsurface of Ni, where the C atom is stabilized. This Pac-Man mechanism can chomp away on the longer hydrocarbon chains as subsequent C's lose their H's. In some cases, a  $C_2$  fragment can be chomped off, when it has been dehydrogenated. These observations suggest that there may be precursor choices that would optimize the C–H and C–C bond breaking rates with surface diffusion rates to control CNT growth. Additionally, the selection of the feedstock precursor might control the extent of carbide formation to take advantage of the role nickel carbide may play in a variety of CNT growth mechanisms.

**Acknowledgment.** This research was supported partly by Intel Components Research and by Intel Corporate Research.

**Supporting Information Available:** Full set of ReaxFF parameters used in these studies, trajectories for RD simulations, hydrocarbon populations as a function of time from RD simulations, and detailed results from analysis of adsorption rates using a kinetic model. This material is available free of charge via the Internet at <http://pubs.acs.org>.

## References and Notes

- (1) Røstrup-Nielsen, J. R. *Catalytic Steam Reforming, in Catalysis, Science and Technology*; Anderson, J. R., Boudar, M., Eds.; Springer: Berlin, 1984; p 1.
- (2) Egeberg, R. C.; Ullman, S.; Alstrup, I.; Mullins, C. B.; Chorkendorff, I. Dissociation of  $CH_4$  on Ni(111) and Ru(0001). *Surf. Sci.* **2002**, 497 (1–3), 183–193.
- (3) Paillet, M.; Jourdain, V.; Phoncharal, P.; Sauvajol, J.-L.; Zahab, A. Versatile Synthesis of Individual Single-Walled Carbon Nanotubes from Nickel Nanoparticles for the Study of their Physical Properties. *J. Phys. Chem. B* **2004**, 108 (44), 17112–17118.
- (4) Lehwald, S.; Ibach, H. Decomposition of Hydrocarbons on Flat and Stepped Ni(111) Surfaces. *Surf. Sci.* **1979**, 89 (1–3), 425–445.
- (5) Mueller, J. E.; van Duin, A. C. T.; Goddard, W. A. *Structures, Energetics, and Reaction Barriers for  $CH_x$  Bound to Ni(111) Surfaces* **2009**, 113 (47), 20290–20306.

- (6) Watwe, R. M.; Bengaard, H. S.; Rostrup-Nielsen, J. R.; Dumesic, J. A.; Norskov, J. K. Theoretical Studies of Stability and Reactivity of  $\text{CH}_x$  species on Ni(111). *J. Catal.* **2000**, *189* (1), 16–30.
- (7) Yang, Q. Y.; Maynard, K. J.; Johnson, A. D.; Ceyer, S. T. The Structure and Chemistry of  $\text{CH}_3$  and CH Radicals Adsorbed on Ni(111). *J. Chem. Phys.* **1995**, *102* (19), 7734–7749.
- (8) Mora, E.; Pigos, J. M.; Ding, F.; Yakobson, B. I.; Harutyunyan, A. R. Low-Temperature Single-Wall Carbon Nanotubes Synthesis: Feedstock Decomposition Limited Growth. *J. Am. Chem. Soc.* **2008**, *130* (36), 11840–11841.
- (9) Demuth, J. E. Conversion of Ethylene to Acetylene on Ni(111). *Surf. Sci.* **1978**, *76* (2), L603–L608.
- (10) Kaminsky, M. P.; Winograd, N.; Geoffroy, G. L. Direct SIMS Observation of Methyldyne, Methylene, and Methyl Intermediates on a Ni(111) Methanation Catalyst. *J. Am. Chem. Soc.* **1986**, *108* (6), 1315–1316.
- (11) Lehwald, S.; Ibach, H.; Demuth, J. E. Vibration Spectroscopy of Benzene Adsorbed on Pt(111) and Ni(111). *Surf. Sci.* **1978**, *78* (3), 577–590.
- (12) Yang, Q. Y.; Johnson, A. D.; Maynard, K. J.; Ceyer, S. T. Synthesis of Benzene from Methane over a Ni(111) Catalyst. *J. Am. Chem. Soc.* **1989**, *111* (23), 8748–8749.
- (13) Car, R.; Parrinello, M. Unified Approach for Molecular-Dynamics and Density-Functional Theory. *Phys. Rev. Lett.* **1985**, *55* (22), 2471–2474.
- (14) Mueller, J. E.; van Duin, A. C. T.; Goddard, W. A. Development and Validation of the ReaxFF Reactive Force Field for Hydrocarbon Chemistry Catalyzed by Nickel. *J. Phys. Chem. C*, submitted for publication.
- (15) Nielson, K. D.; van Duin, A. C. T.; Oxgaard, J.; Deng, W. Q.; Goddard, W. A. Development of the ReaxFF Reactive Force Field for Describing Transition Metal Catalyzed Reactions, with Application to the Initial Stages of the Catalytic Formation of Carbon Nanotubes. *J. Phys. Chem. A* **2005**, *109* (3), 493–499.
- (16) Dai, H. J.; Rinzler, A. G.; Nikolaev, P.; Thess, A.; Colbert, D. T.; Smalley, R. E. Single-Wall Nanotubes Produced by Metal-Catalyzed Disproportionation of Carbon Monoxide. *Chem. Phys. Lett.* **1996**, *260* (3–4), 471–475.
- (17) Fylstra, D.; Lasdon, L.; Watson, J.; Waren, A. Design and Use of the Microsoft Excel Solver. *Interfaces* **1998**, *28* (5), 29–55.
- (18) Yang, Q. Y.; Ceyer, S. T. The Stability and Chemistry of Methyl Radicals Adsorbed on Ni(111). *J. Vac. Sci. Technol., A* **1988**, *6* (3), 851–852.
- (19) Henkelman, G.; Arnaldsson, A.; Jonsson, H. Theoretical Calculations of  $\text{CH}_4$  and  $\text{H}_2$  Associative Desorption from Ni(111): Could Subsurface Hydrogen Play an Important Role? *J. Chem. Phys.* **2006**, *124* (4), 044706.
- (20) Michaelides, A.; Hu, P. A First Principles Study of  $\text{CH}_3$  Dehydrogenation on Ni(111). *J. Chem. Phys.* **2000**, *112* (18), 8120–8125.
- (21) Bao, S.; Hofmann, Ph.; Schindler, K.-M.; Fritzsche, V.; Bradshaw, A. M.; Woodruff, D. P.; Casado, C.; Asenio, M. C. The Local Geometry of Reactant and Product in a Surface-Reaction: the Dehydrogenation of Adsorbed Ethylene on Ni(111). *Surf. Sci.* **1995**, *323* (1–2), 19–29.
- (22) Demuth, J. E. Molecular Geometries of Acetylene and Ethylene Chemisorbed on Cu, Ni, Pd, and Pt Surfaces. *IBM J. Res. Dev.* **1978**, *22* (3), 265–276.
- (23) Demuth, J. E.; Eastman, D. E. Determination of State of Hybridization of Unsaturated-Hydrocarbons Chemisorbed on Nickel. *Phys. Rev. B* **1976**, *13* (4), 1523–1527.
- (24) Demuth, J. E.; Eastman, D. E. Photoemission Observations of  $\pi$ -d Bonding and Surface Reactions of Adsorbed Hydrocarbons on Ni(111). *Phys. Rev. Lett.* **1974**, *32* (20), 1123–1127.
- (25) Demuth, J. E.; Ibach, H.; Lehwald, S. CH Vibration Softening and Dehydrogenation of Hydrocarbon Molecules on Ni(111) and Pt(111). *Phys. Rev. Lett.* **1978**, *40* (15), 1044–1047.
- (26) Sham, T. K.; Carr, R. G. Carbon Near Edge X-Ray Absorption Fine-Structure (NEXAFS) Studies of Ethylene Adsorption on Ni(111) and Ni(110) Surfaces: Implication for Surface-Morphology Insensitive Reactions. *J. Chem. Phys.* **1986**, *84* (7), 4091–4095.
- (27) Zhu, X. Y.; Castro, S.; Akhter, S.; White, J. M.; Houston, J. E. Static Secondary Ion Mass-Spectroscopy Study of Ethylene and Acetylene on Ni: Coverage Dependence. *J. Vac. Sci. Technol., A* **1989**, *7* (3), 1991–1995.
- (28) Zhu, X. Y.; White, J. M. Interaction of Ethylene and Acetylene with Ni(111): A SSIMS Study. *Surf. Sci.* **1989**, *214* (1–2), 240–256.
- (29) Anderson, A. B. Structural and Orbital Analysis of Ethylene and Acetylene on Ni(111) Surfaces. *J. Chem. Phys.* **1976**, *65* (5), 1729–1734.
- (30) Fahmi, A.; van Santen, R. A. Density Functional Study of Acetylene and Ethylene Adsorption on Ni(111). *Surf. Sci.* **1997**, *371* (1), 53–62.
- (31) Medlin, J. W.; Allendorf, M. D. Theoretical Study of the Adsorption of Acetylene on the (111) Surfaces of Pd, Pt, Ni, and Rh. *J. Phys. Chem. B* **2003**, *107* (1), 217–223.
- (32) Pac-Man is a character in the Pac-Man arcade game first produced by Namco in 1980. Pac-Man is represented as a yellow circle (or sphere) with a wedged shaped mouth that continually opens and closes as he moves through a maze eating Pac-dots one at a time. In an analogous manner, the Ni particle breaks C–C bonds by “eating up” the C atoms one at a time in what we call the Pac-Man mechanism.
- (33) Bertolini, J. C.; Rousseau, J.  $\text{C}_2\text{H}_4$  Adsorption on the Ni(111) Face at Room-Temperature: Vibrations of Surface Complexes Studied by Electron-Energy Loss Spectroscopy. *Surf. Sci.* **1979**, *83* (2), 531–544.
- (34) Demuth, J. E. Interaction of Acetylene with Ni(111), Chemisorbed Oxygen on Ni(111), and NiO(111): Formation of CH Species on Chemically Modified Ni(111) Surfaces. *Surf. Sci.* **1977**, *69* (2), 365–384.
- (35) Demuth, J. E. Structure of Chemisorbed Acetylene and Ethylene on Ni, Pd and Pt Surfaces. *Surf. Sci.* **1979**, *84* (2), 315–328.
- (36) Demuth, J. E.; Ibach, H. Experimental Study of the Vibrations of Acetylene Chemisorbed on Ni(111). *Surf. Sci.* **1979**, *85* (2), 365–378.
- (37) Demuth, J. E.; Ibach, H. Identification of CH Species on Ni(111) by High-Resolution Electron-Energy Loss Spectroscopy. *Surf. Sci.* **1978**, *78* (1), L238–L244.
- (38) Mittendorfer, F.; Hafner, J. Density-Functional Study of the Adsorption of Benzene on the (111), (100) and (110) Surfaces of Nickel. *Surf. Sci.* **2001**, *472* (1–2), 133–153.
- (39) Goddard, W. A.; Carter, E. A.; Guo, Y.; Peters, J. C.; Donnelly, R. E.; Low, J. J. Chemisorbed Intermediates on Metal and Semiconductor Surfaces. *Abs. Pap. Am. Chem. Soc.* **1987**, *194*, 85. -Phys.
- (40) Rodriguez-Manzo, J. A.; Terrones, M.; Terrones, H.; Kroto, H. W.; Sun, L.; Banhart, F. In situ Nucleation of Carbon Nanotubes by the Injection of Carbon Atoms into Metal Particles. *Nat. Nanotechnol.* **2007**, *2* (5), 307–311.
- (41) Saito, Y. Nanoparticles and Filled Nanocapsules. *Carbon* **1995**, *33* (7), 979–988.
- (42) Wagner, R. S.; Ellis, W. C. Vapor-Liquid-Solid Mechanism of Single Crystal Growth. *Appl. Phys. Lett.* **1964**, *4* (5), 89–90.
- (43) Hofmann, S.; Csanyi, G.; Ferrari, A. C.; Payne, M. C.; Robertson, J. Surface Diffusion: The Low Activation Energy Path for Nanotube Growth. *Phys. Rev. Lett.* **2005**, *95* (3), 036101.
- (44) Ding, F.; Bolton, K.; Rosen, A. Nucleation and Growth of Single-Walled Carbon Nanotubes: A Molecular Dynamics Study. *J. Phys. Chem. B* **2004**, *108* (45), 17369–17377.
- (45) Ding, F.; Rosen, A.; Bolton, K. Molecular Dynamics Study of the Catalyst Particle Size Dependence on Carbon Nanotube Growth. *J. Chem. Phys.* **2004**, *121* (6), 2775–2779.
- (46) Ding, F.; Rosen, A.; Bolton, K. The Role of the Catalytic Particle Temperature Gradient for SWNT Growth from Small Particles. *Chem. Phys. Lett.* **2004**, *393* (4–6), 309–313.
- (47) Maiti, A.; Brabec, C. J.; Bernholc, J. Kinetics of Metal-Catalyzed Growth of Single-Walled Carbon Nanotubes. *Phys. Rev. B* **1997**, *55* (10), R6097–R6100.
- (48) Maiti, A.; Brabec, C. J.; Roland, C.; Bernholc, J. Theory of Carbon Nanotube Growth. *Phys. Rev. B* **1995**, *52* (20), 14850–14858.
- (49) Shibuta, Y.; Maruyama, S. Molecular Dynamics Simulation of Formation Process of Single-Walled Carbon Nanotubes by CCVD Method. *Chem. Phys. Lett.* **2003**, *382* (3–4), 381–386.
- (50) Shibuta, Y.; Maruyama, S. Molecular Dynamics Simulation of Generation Process of SWNTs. *Physica B* **2002**, *323* (1–4), 187–189.
- (51) Abild-Pedersen, F.; Norskov, J. K.; Rostrup-Nielsen, J. R.; Sehested, J.; Helveg, S. Mechanisms for Catalytic Carbon Nanofiber Growth Studied ab initio Density Functional Theory Calculations. *Phys. Rev. B* **2006**, *73* (11), 115419.
- (52) Amara, H.; Bichara, C.; Ducastelle, F. Understanding the Nucleation Mechanisms of Carbon Nanotubes in Catalytic Chemical Vapor Deposition. *Phys. Rev. Lett.* **2008**, *100* (5), 056105.
- (53) Bengaard, H. S.; Norskov, J. K.; Sehested, J.; Causen, B. S.; Nielsen, L. P.; Molenbroek, A. M.; Rostrup-Nielsen, J. R. Steam Reforming and Graphite Formation on Ni Catalysts. *J. Catal.* **2002**, *209* (2), 365–384.
- (54) Hofmann, S.; Sharma, R.; Ducati, C.; Du, G.; Mattevi, C.; Cepek, C.; Cantoro, M.; Pisana, S.; Parvez, A.; Cervantes-Sodi, F.; Ferrari, A. C.; Dunin-Borkowski, R.; Lizzit, S.; Petaccia, L.; Goldoni, A.; Robertson, J. In situ Observations of Catalyst Dynamics during Surface-Bound Carbon Nanotube Nucleation. *Nano Lett.* **2007**, *7* (3), 602–608.